Figure S1. Effects of CD46 on the regulation of migratory in 253J cell. Bright-field images showing scratched areas (marked by red lines) in confluent monolayers of cancer cell overexpressing CD46 at different time points (left panel). Relative wound closure was assessed by measuring the width of the wounds compared with control cells (right panel). Each bar represents mean ± SD. Scale bars, 200 μm. Differences between groups were assessed using a paired two-tailed Student's t-test. $^{ns}P>0.05$ vs. control cells. veh, vehicle.

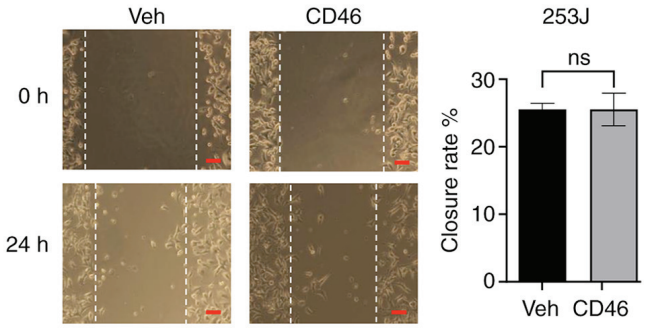

Figure S2. Effects of CD46 siRNA on the regulation of migratory and invasive potential in bladder cancer cells. (A) Bright-field images showing scratched areas (marked by white lines) in confluent monolayers of cancer cells suppressing CD46 at different time points (left panel). Relative wound closure was assessed by measuring the width of the wounds compared with control cells (right panel). (B) Transwell assays to measure cell migration and invasion in 5637 cells transfected with CD46 siRNA (left panel). Quantification of cell migration and invasion was conducted (right panel). Each bar represents mean ± SD. Scale bars, 200 μm. Differences between groups were assessed using a two-tailed unpaired Student's t-test. *P<0.01, **P<0.001, ***P<0.0001 vs. control cells. si, short interfering.

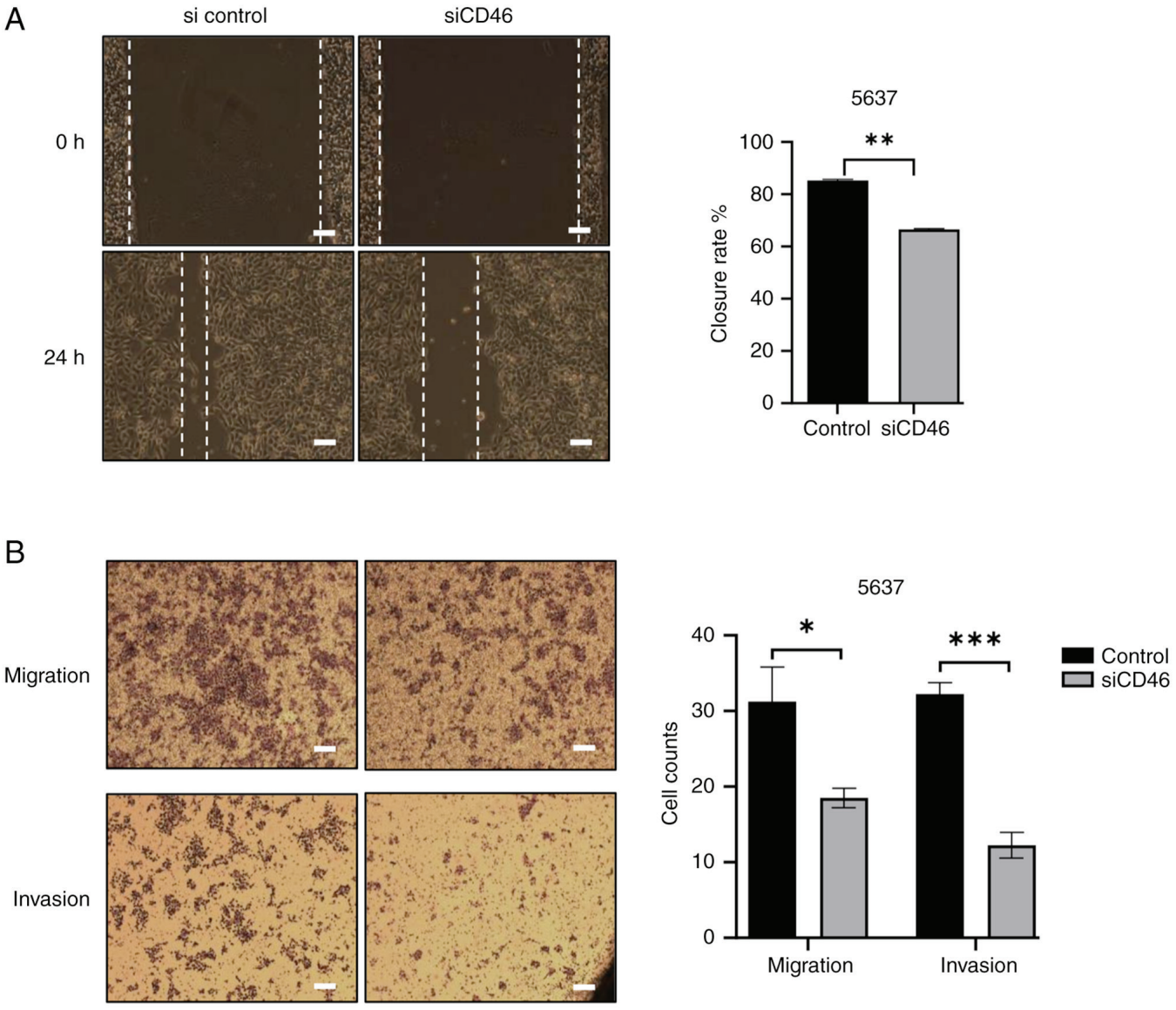

Figure S3. Effects of CD46 on experimental lung metastasis in a murine bladder cancer model. (A) After cell injection, weight of mice were checked each week up to 6 weeks and are illustrated. (B) Mice injected with either 5637 or UM-UC-3 cells are shown at the sacrifice time. (C) Optical fluorescent images of lung metastasis for athymic nude mice injected with 5637-veh and 5637-CD46 cells. (D) Histological images of lungs obtained from mice injected with 5637-veh and 5637-CD46 cells. Scale bars, 2 mm. P-values were obtained using the U-Mann Whitney test ($^{ns}P>0.05$).